Analysis of binning of normals for spherical harmonic cross-correlation

Robert L. Larkins, Michael J. Cree, and Adrian A. Dorrington

School of Engineering, University of Waikato
Private Bag 3105, Hamilton 3240, New Zealand

ABSTRACT

Spherical harmonic cross-correlation is a robust registration technique that uses the normals of two overlapping point clouds to bring them into coarse rotational alignment. This registration technique however has a high computational cost as spherical harmonics need to be calculated for every normal. By binning the normals, the computational efficiency is improved as the spherical harmonics can be pre-computed and cached at each bin location. In this paper we evaluate the efficiency and accuracy of the equiangle grid, icosahedron subdivision and the Fibonacci spiral, an approach we propose. It is found that the equiangle grid has the best efficiency as it can perform direct binning, followed by the Fibonacci spiral and then the icosahedron, all of which decrease the computational cost compared to no binning. The Fibonacci spiral produces the highest achieved accuracy of the three approaches while maintaining a low number of bins. The number of bins allowed by the equiangle grid and icosahedron are much more restrictive than the Fibonacci spiral. The performed analysis shows that the Fibonacci spiral can perform as well as the original cross-correlation algorithm without binning, while also providing a significant improvement in computational efficiency.

Keywords: spherical harmonics, cross-correlation, registration, point-cloud, normal binning, Fibonacci spiral

1. INTRODUCTION

The registration of overlapping point clouds has recently received increased attention due to the growing availability of systems capable of range data acquisition.[1] If there is no method of tracking how the camera or object moves, then the rotational and translational change between image captures is a priori unknown. There are a variety of registration algorithms capable of aligning overlapping point clouds, such as iterative closest point (ICP), RANSAC, and principal component analysis. These are summarized well by Salvi et al.[2]

The focus of this paper is on spherical cross-correlation, which achieves coarse rotational alignment while remaining robust to noise. This alignment is performed by taking the normal from every vertex of both point clouds and converting them to spherical harmonics. The cross-correlation then uses the spherical harmonics to identify a rotation that maximises rotational alignment. The computational cost of calculating the spherical harmonics is determined by the total number of harmonics that are calculated, which depends upon the desired rotation precision and the number of normals. Fortunately, this cost can be mitigated by performing the cross-correlation on a histogram of the normals.

Normals are represented by unit vectors, and therefore specify a direction out from the origin of the coordinate system, identifying a point on the surface of a unit sphere. A histogram of the normals can be performed on the sphere surface by breaking it into bins that collect the normals. The computational advantage that this provides is that the bin locations can be defined and their spherical harmonics pre-computed, with the weight of each bin being applied to their respective set of harmonics. The cost of spherical harmonic calculation is removed as the processing is shifted to the binning instead.

The first use of spherical cross-correlation for registering 3D data[3] did not form a histogram of the normals, instead performed an exhaustive search at 5° increments of the spherical harmonics. Pre-computation of the

Further author information: (Send correspondence to R.L.L.)
R.L.L.: E-mail: rll6@students.waikato.ac.nz
M.J.C.: E-mail: cree@waikato.ac.nz
A.A.D.: E-mail: adrian@waikato.ac.nz

Three-Dimensional Image Processing (3DIP) and Applications II, Edited by Atilla M. Baskurt, Robert Sitnik, Proc. of SPIE 8290, 82900L, 2012
http://dx.doi.org/10.1117/12.909466

spherical harmonics improves performance, but using a grid of equally spaced polar coordinates, referred to as an equiangle grid, is not optimal due to the decreased point density at the equator, therefore an icosahedral based approach was better for matching a pair of macromolecular surface shapes.[4] Nevertheless if speed is a priority then an equiangle grid approach may be a better choice for fast correlation.[5] Registration by performing a hierarchical search in which each subsequent depth of an icosahedron identifies a set of localised bins to use for the cross-correlation to improve the registration accuracy,[6] however, this method is an iterative search. We are not aware of any comparative investigations of the effect of different binning techniques on spherical cross-correlation.

The work presented here investigates the performance of three different binning approaches and how they impact the registration ability of spherical cross-correlation. The equiangle grid and icosahedron approaches have been used previously, while a third approach that uses a Fibonacci spiral point distribution[7] for positioning bins is introduced here as an alternative for normal binning. The goal of this analysis is to identify the efficiency of these approaches as well as their ability to minimise the resulting angle error. From this analysis the ideal solution is one that minimises the number of bins required while producing an angle error that is as close to or the same as what the spherical cross-correlation produces without binning.

In Section 2 the three binning approaches are described and their implementations outlined, while Section 3 gives the mathematical preliminaries for the spherical cross-correlation. The methodology, results and discussion of the analysis are covered in Sections 4, 5, and 6, respectively. The paper is then concluded in Section 7.

2. BINNING APPROACHES

A captured point cloud provides a sampling of a surface where each vertex has an associated normal which points away from this surface. The relationship between normals remains the same, allowing the rotational alignment of two point clouds to be found no matter how they are shifted with respect to each other. Extracting the normals from the point cloud means that they are no longer associated with a vertex on the surface, and become unit vectors that specify a direction out from the origin, and can therefore be binned in

$$\mathbb{S}^2 = \left\{ x \in \mathbb{R}^3 : ||x|| = 1 \right\}. \tag{1}$$

Binning in $\mathbb{S}^2$ is equivalent to dividing the surface of a unit sphere in a regular fashion and is referred to as the Fekete problem or Tamme's problem, and has many proposed solutions,[8–12] none of which can be considered the single best method.

For the task of spherical cross-correlation, three methods of point distribution for normal binning are investigated. Equiangle grid and icosahedron have been reported previously for use in spherical correlation,[5,6] while the Fibonacci spiral is explored herein for the first time. Figures 1a, 1b and 1c show the distribution of points, with bin boundaries presented in Figures 1d, 1e and 1f, respectively. The number of normals each bin collects forms its weight. The center of each bin is stored as a spherical coordinate which along with its collected weight provides the necessary components for performing spherical cross-correlation.

2.1 Equiangle Grid

An equiangle grid is the simplest approach for dividing the sphere into bins, and has been used previously in conjunction with spherical harmonic registration.[5] The bins are created by dividing the polar angle θ and the azimuthal angle ϕ equally. Let d be the number of divisions and the top left corner of each bin, b, be given by the spherical coordinates,

$$b_{v,h} = \left[\frac{v\pi}{d}, \frac{h\pi}{d} \right], \qquad v \in 0, \ldots, d-1, \qquad h \in 0, \ldots, 2d-1, \tag{2}$$

where v and h index the bins. Any normal that falls within the boundaries of a bin increases the weight of that bin. The centers of the bins are given by,

$$B_{v,h} = \left[\frac{\pi(2v-1)}{2d}, \frac{\pi(2h-1)}{2d} \right], \qquad v \in 0, \ldots, d-1, \qquad h \in 0, \ldots, 2d-1. \tag{3}$$

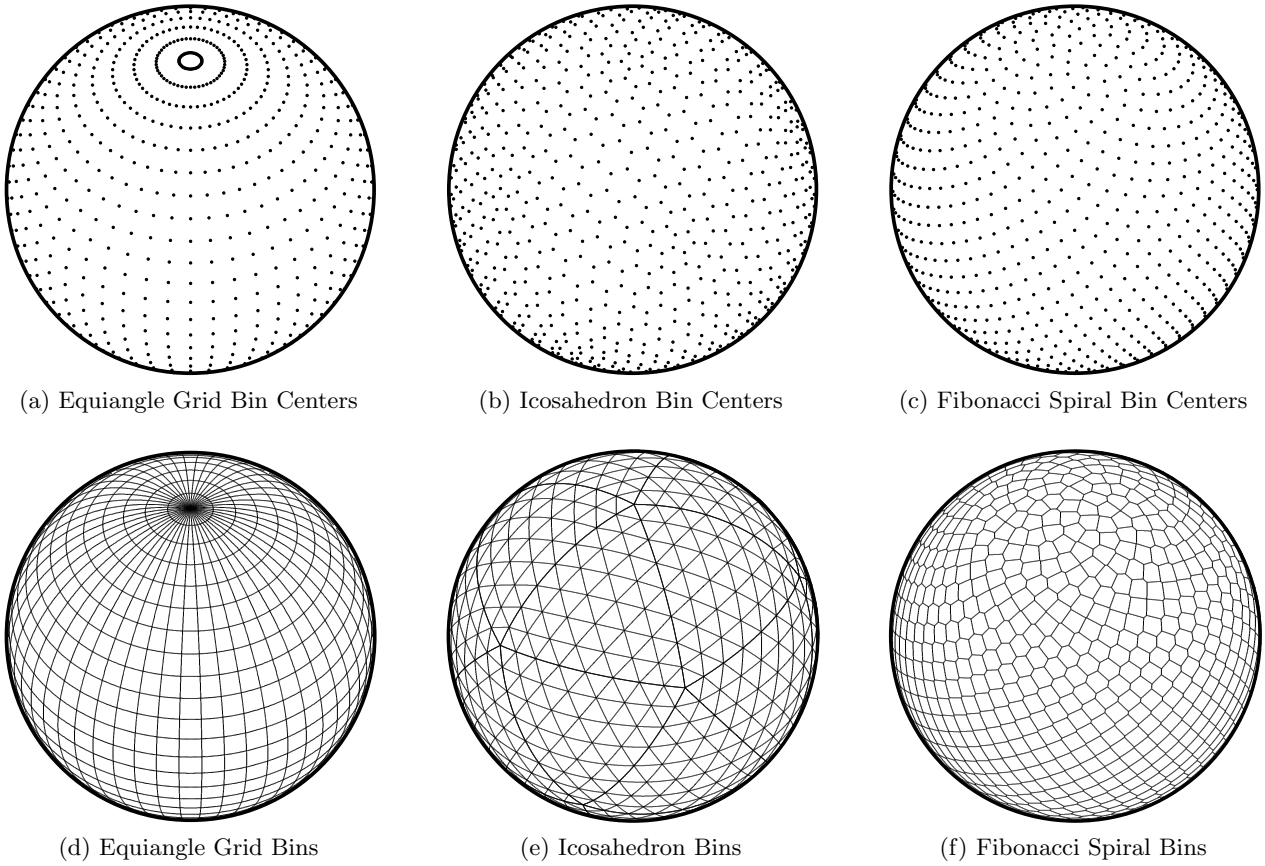

(a) Equiangle Grid Bin Centers (b) Icosahedron Bin Centers (c) Fibonacci Spiral Bin Centers

(d) Equiangle Grid Bins (e) Icosahedron Bins (f) Fibonacci Spiral Bins

Figure 1: Orthographic projection of spheres displaying the three binning methods; the spheres are tilted 45° making the north pole visible. The top row shows the distribution of the bin centers, while the bottom row shows the bin boundaries. The number of bins distributed about each sphere are 1250, 1280 and 1281, for the equiangle grid, icosahedron and Fibonacci spiral, respectively.

The equiangle grid has a total of $n = 2d^2$ bins. The placement of the bins on the unit sphere is illustrated in Figure 1d. Note the increased density of bins towards the poles, with a reduction in bin surface area.

Implementation

By equally sampling the polar and azimuthal angles, the bin that a normal belongs to can be directly calculated without relying on any form of searching. The integers v and h that specify the bin are found from a normal, $N = (N_\theta, N_\phi)$, as

$$v = \begin{cases} \left\lfloor \frac{dN_\theta}{\pi} \right\rfloor & \text{if} \quad 0 \le N_\theta < \pi, \\ d - 1 & \text{if} \quad N_\theta = \pi; \end{cases} \tag{4}$$

$$h = \begin{cases} \left\lfloor \frac{dN_\phi}{\pi} \right\rfloor & \text{if} \quad 0 \le N_\phi < 2\pi, \\ 0 & \text{if} \quad N_\phi = 2\pi. \end{cases} \tag{5}$$

Given v and h, equation (3) gives the bin that a normal N belongs to.

2.2 Geodesic Subdivision

Geodesic subdivision is achieved by centering a Platonic solid at the origin of the coordinate system and projecting each face on to the surface of a unit sphere to form a bin.[10] The icosahedron is typically used as it has the most faces of the five Platonic solids. As each face of the icosahedron is an equilateral triangle, more bins can

be formed by breaking each face into four subsequent equilateral triangular regions, with this process repeated to a preferred depth; as seen in Figure 1e where the icosahedron has a depth of three.

The locations of the twelve vertices of the icosahedron on the unit sphere can be expressed in terms of the golden ratio,

$$\tau = \frac{1+\sqrt{5}}{2}, \tag{6}$$

which if aligned with a vertex at each pole are (in Cartesian coordinates):

$$\begin{bmatrix} 0 & 0 & \pm 1 \\ \pm 2/\sqrt{5} & 0 & \mp(2/(\tau^2+1)-1) \\ \pm 1/(\tau^2+1) & \pm 1/\sqrt{\tau^{-2}+1} & \pm 1/\sqrt{5} \\ \pm 1/(\tau^2+1) & \mp 1/\sqrt{\tau^{-2}+1} & \pm 1/\sqrt{5} \\ \mp 1/(\tau^{-2}+1) & \mp 1/\sqrt{\tau^2+1} & \pm 1/\sqrt{5} \\ \mp 1/(\tau^{-2}+1) & \pm 1/\sqrt{\tau^2+1} & \pm 1/\sqrt{5} \end{bmatrix}. \tag{7}$$

These vertices are presented in pairs that occur directly opposite each other on the sphere. The 20 faces defined by these vertices are projected onto the sphere, creating the initial bins. By specifying a depth, d, more bins can be produced by subsequently dividing each face into four smaller equilateral triangles and projecting these on to the sphere surface. The number of bins is given by

$$n = 20 \times 4^d. \tag{8}$$

Each face of the icosahedron is split into a total of 4^d triangles which become bins when projected onto the sphere surface. However, this projection changes the size and shape of each bin. Bins closer to the center of each face have a greater surface area than those at the edge, thus there is a higher density of bin centers at the edges. This change in density impacts the following implementation as the best branch to traverse at a lower depth may not contain the ideal bin, placing the normal in a bin adjacent to the ideal bin. It has been stated, though unconfirmed, that for most practical purposes this slight bias is insignificant.[9] This claim is further investigated as part of this study.

Implementation

Binning normals using geodesic subdivision is done in two stages. The first is to build the tree that stores the bins at each depth, and the second is to search down the tree to find the closest bin.

The bin tree is constructed as 20 individual trees, one for each face, where each face is defined by three vertices from those listed in equation (7). The center of this face is then projected onto the sphere surface by normalizing its magnitude to 1. This normalized face center is then stored as a spherical coordinate in the root node of the corresponding tree. For every new level, each node has four children, one for each of the four subsequent triangles that are created. The centers of these new triangles are normalized and stored as spherical coordinates. This forms a quad-tree, that is stored as a linear array, with the index of each child node, i_c, found from the index of the parent node, i_p, by

$$i_c = 4i_p + c, \qquad c \in \{1,2,3,4\}. \tag{9}$$

Each tree contains t nodes, given by

$$t = \frac{4^{d+1}-1}{3}, \tag{10}$$

where d is the depth of the tree. Composing a linear array that only stores the leaf nodes and their weights from all 20 trees can be achieved, where the index, i_b, of a bin in this array is found by

$$i_b = 4^d(f - 3^{-1}) + i_l + 3^{-1}, \qquad f \in \{0,\ldots,19\}, \tag{11}$$

where f is the face and i_l is the index of the leaf node in the above mentioned quad-tree.

The bin that a normal belongs to is found by first identifying which of the 20 faces, or zero depth bins it is closest to. As the normals and bins represent a position on a unit sphere, the great circle distance (GCD) is the same as the angle between the normal, $N_{[\theta,\phi]}$, and the center of a bin, $B_{[\theta,\phi]}$, calculated as

$$\psi = \cos^{-1}\left(\sin N_\theta \sin B_\theta \cos\left(N_\phi - B_\phi\right) + \cos N_\theta \cos B_\theta\right). \tag{12}$$

The layout of the vertices of the icosahedron produces pairs of root nodes that are on direct opposite sides of the unit sphere. The distance therefore needs to be calculated for only ten of the nodes, and the distance of a node's counterpart is given by $\pi - \psi$. If a single shortest distance is found, then the normal goes to the corresponding root node and the search down the tree for the wanted bin begins.

Given the closest root node, the distance between its four children and the normal is found using equation (12). This process of finding the closest node and going down its branch is repeated until a leaf node is reached; with the spherical coordinate of the leaf node being the closest bin. Using equation (11) the weight of this bin is then incremented. Throughout this process, both for finding the root node and for searching down the quad-tree, there is the unlikely possibility that a normal is located where multiple nodes have the same shortest distance, in this situation, one of these closest nodes is arbitrarily chosen and used.

2.3 Fibonacci Spiral

The Fibonacci spiral[7] is a point distribution method that we propose as an alternative approach for binning normals. A spiral is created around the sphere from the north to south pole, with each point placed at equal increments along the spiral, creating a distribution like that in Figure 1c which is a near uniform distribution of bin centers around the sphere. The bin boundaries then form around each point, as shown in Figure 1f. An odd number of points must be along the spiral to ensure both hemispheres contain the same number of bin centers. Using the number of bins, n, the bin centers are then found as spherical coordinates at

$$B_{[\theta,\phi]}\left(d\right) = \left[\sin^{-1}\left(\frac{2d}{n}\right) + \frac{\pi}{2},\ \frac{2\pi}{\tau} \bmod \left(d, \tau\right)\right], \qquad d \in \frac{1-n}{2}, \ldots, \frac{n-1}{2}. \tag{13}$$

Implementation

The binning of normals on a Fibonnaci spiral distribution can potentially be achieved in a variety of ways such as brute force calculation or by a form of Delaunay triangulation. Here we introduced a new algorithm that uses the turns of the spiral to identify bins a normal may belong to, reducing the number of evaluations of equation (12). This is achieved by finding the location on each turn that has the same azimuthal angle as the normal, with the point closest to this location being the closest bin center for that turn. By giving each turn an integer value Z, the spherical coordinate location on each turn can be found by

$$T_{[\theta,\phi]}\left(Z\right) = \left[\sin^{-1}\left(\frac{-\left(Z + v_2\right)}{v_1}\right) + \frac{\pi}{2},\ N_\phi\right], \qquad Z \in Z_{\min}, \ldots, Z_{\max}, \tag{14}$$

where $Z_{\min} = \lceil -v_1 - v_2 \rceil$ and $Z_{\max} = \lfloor v_1 - v_2 \rfloor$, when given $v_1 = n/(2\tau^2)$ and $v_2 = N_\phi/(2\pi)$, constant variables common throughout these equations. The closest bin center to $T\left(Z\right)$ on that turn is found via equation (13) when

$$d = \text{round}\left(-\tau^2\left(Z + v_2\right)\right). \tag{15}$$

The searching begins by first testing the turn on either side of the normal, in which the bin center with the smallest distance, ψ, of these two turns is stored. The Z value of the normal is given as a real value and is found as

$$Z = v_1 \times \sin\left(N_\theta - \frac{\pi}{2}\right) - v_2, \tag{16}$$

with the two closest turns being identified by taking the floor and ceiling of the calculated Z value. Having done these two tests, each successive turn away from the normal is tested, both going up and down the sphere. If the distance from the normal to T is greater than the current smallest distance, the bin center on this turn is tested and then the stepping in this direction is stopped.

Because the turns of the spiral have a greater spacing towards the poles, the above approach may miss the ideal bin center, therefore, when the normal is above the spiral or there is only one turn above it, that is, when $N_\theta < T_\theta\,(Z_{\min}+1)$, all bin centers from the closest turn location up must be tested. Once this is done, searching down the spiral is carried out as described above. This process is repeated by testing all bin centers down the spiral when $N_\theta > T_\theta\,(Z_{\max}-1)$, followed by testing each turn up the spiral.

This implementation requires two full turns of the spiral to operate correctly, which only occurs when there are 7 or more bins. When the number of bins is 1, 3 or 5, it is feasible to find the distance to every bin. We are interested in a far greater number of bins, hence the need for the search.

3. REGISTRATION PRELIMINARIES

Having formed the histograms of the normals of two points clouds, the bin centers and their associated weighting are used to determine the rotation that brings the second point cloud into rotational alignment with the first. Once the rotational alignment is achieved, the translational alignment can be calculated. This section covers the mathematical preliminaries of spherical cross-correlation for point cloud registration.

3.1 Rotational Alignment

The spherical cross-correlation produces an alignment rotation by correlating two histograms of surface normals.[5,6,13] Because the bin centers are defined over $\mathbb{S}^2$, the transformation to the Fourier domain is carried out using associated Legendre polynomials, to produce a set of spherical harmonic functions that represent the weighted bin centers in the frequency domain. Let P_l^m be the associated Legendre polynomial of degree l with $l \in 0,\ldots,L$ and L the maximum degree, and of order m with $m \in -l,\ldots,l$. The spherical harmonics of a histogram bin with center $B = B_{[\theta,\phi]}$ and weight B_ω, are given by

$$Y_l^m(B) = \begin{cases} \sqrt{\frac{(2l+1)(l-m)!}{4\pi(l+m)!}}\,P_l^m(\cos B_\theta)e^{imB_\phi}B_\omega & m \geq 0, \\ (-1)^m\overline{Y_l^{|m|}\,(B)} & m < 0, \end{cases} \tag{17}$$

where $\overline{x}$ is the complex conjugate of x. Using n bin centers and their corresponding histogram of normals f from the first point cloud, the spherical harmonic representation of f is found as

$$\hat{f}_l^m = \sum_{j=0}^{n-1} Y_l^m(B_j), \tag{18}$$

with the analogous operation applied to the histogram of normals g of the second point cloud to give $\hat{g}$. The Fourier transform of the three-dimensional rotation correlation matrix, $\hat{C}_R$, between $\hat{f}$ and $\hat{g}$ is given by

$$\hat{C}_R(m,n,k) = \sum_{l=\max(|m|,|n|,|k|)}^{L} \overline{\hat{f}_l^n}\hat{g}_l^m d_{mk}^l d_{kn}^l, \qquad m,n,k \in -L,\ldots,L \tag{19}$$

The function d is a necessary component for performing a rotation on spherical harmonics. The version of d presented here,

$$d_{mn}^l = 2^{-l} \sum_{t=\max(0,n-m)}^{\min(l+n,l-m)} (-1)^t \times \frac{\sqrt{(l+n)!(l-n)!(l+m)!(l-m)!}}{(l+n-t)!(l-m-t)!(t+m-n)!t!}, \tag{20}$$

is a simplified version of that found in Ref. 13, and provides an elegant approach for spherical cross-correlation.[4]

The final step is to apply the inverse Fourier transform to $\hat{C}_R$ to obtain the correlation matrix, C_R. The maximum impulse response in C_R identifies the rotation that gives the best overlap of the two sets of normals.

Taking a, b and c as the indices of the maximum value of C_R then the Euler angles α, β and γ are found by

$$\alpha = \mathrm{mod}\left(\frac{2\pi(a+L)}{2L+1} + \frac{\pi}{2},\ 2\pi\right), \tag{21}$$

$$\beta = \mathrm{mod}\left(\frac{2\pi(b+L)}{2L+1} + \pi,\ 2\pi\right), \tag{22}$$

$$\gamma = \mathrm{mod}\left(\frac{2\pi(c+L)}{2L+1} + \frac{\pi}{2},\ 2\pi\right). \tag{23}$$

Applying these angles to a ZYZ rotation matrix will generally bring the two point clouds into rotational alignment.

3.2 Translational Alignment

Once the two overlapping point clouds are in rotational alignment, the translational alignment is easily found by a Fourier phase correlation of the point clouds. The two point clouds are first shifted so that their centroids are located at the origin of the coordinate system. To enable use of the conventional discrete Fourier transform even though the points are unevenly spaced, the domain is divided into even sized bins on a Cartesian grid. This formation is centered at the origin, with a side length l and an odd number of bins s placed along each dimension. The weight of each bin is the number of points of the cloud that are located within the bin boundaries. Taking F and G to be the point cloud histograms, with $\hat{F}$ and $\hat{G}$ their respective Fourier transforms, the Fourier phase correlation of the point cloud histograms is given by

$$\hat{C}_T = \frac{\hat{F}\overline{\hat{G}}}{\|\hat{F}\overline{\hat{G}}\|}. \tag{24}$$

The translation correlation matrix C_T is easily obtained by the the inverse Fourier transform of $\hat{C}_T$. The location of the maximum impulse response given by the coordinate (a, b, c) identifies the translation with the best overlap. The translational shift is performed along each axis, where a, b, and c correspond to the x, y, and z directions respectively, and are found as,

$$x = \begin{cases} al/s & a \le (s-1)/2 \\ al/s - l & a > (s-1)/2, \end{cases} \tag{25}$$

$$y = \begin{cases} bl/s & b \le (s-1)/2 \\ bl/s - l & b > (s-1)/2, \end{cases} \tag{26}$$

$$z = \begin{cases} cl/s & c \le (s-1)/2 \\ cl/s - l & c > (s-1)/2. \end{cases} \tag{27}$$

This procedure brings the two point clouds into coarse alignment.

4. METHODOLOGY

The Dragon, Buddha statue, and Stanford bunny, shown in Figure 2, from the Stanford 3D scanning repository*, are used for testing the binning of normals, with each containing 22 982, 32 328, and 35 947 vertices, respectively. From each model a dataset is formed by breaking it into overlapping segments, where a segment is the section of the model visible from a single point-of-view. By shifting the point-of-view around the model at 2° increments, 180 segments are created, giving an exact angle of separation between segments. Each segment and its normals are generated using Blender†.

*http://graphics.stanford.edu/data/3Dscanrep/.

†Blender is an open-source 3D graphics editor (http://www.blender.org/). Version 2.59.0 r39307 is used here.

(a) Dragon (b) Buddha Statue (c) Stanford Bunny

Figure 2: The three models from the Stanford 3D scanning repository used for testing.

A pair of segments are selected for testing if their angle of separation is 50° or less. A coordinate transformation is then applied to both segments shifting their points into the coordinate system of their respective cameras. The spherical cross-correlation is then applied to one of the point clouds to bring it into rotational alignment with the other. Because the chosen spherical harmonic degree produces a discretized correlation matrix, there is a fixed set of potential solutions, and as such, an error in rotational alignment will likely remain. This error is determined as the angle between the found position of the point cloud and its known true position.

The spherical cross-correlation precision is dependent on the maximum degree of Legendre polynomial used and the amount of overlap between two segments. For testing, a maximum degree of 20 is used as this creates enough spherical harmonics so that the resulting angle error is low, whilst still maintaining a reasonable computational efficiency. The amount of overlap between segments is often dependent on their separation angle, therefore to ensure that the testing is broad enough, it is performed on segment pairs that have a separation of up to 50°. This produces 4 355 individual tests per model, with $(180° - \theta/2)$ tests per angle, where θ is the smallest angle of rotation between the segments.

The icosahedron binning only has three feasible bin counts, thus to keep the comparison fair the number of bins used in the equiangle grid and Fibonacci spiral are matched as closely as possible, creating the three bin sets listed in Table 1. The ground truth for these approaches is performing the spherical cross-correlation without binning.

Table 1: The number of bins in the three bin sets for each binning approaches.

Binning Approach	Set 1	Set 2	Set 3
Equiangle Grid	72	338	1250
Icosahedron	80	320	1280
Fibonacci Spiral	79	319	1279

5. RESULTS

The results presented investigate how the efficiency and accuracy are affected by binning the normals. The efficiency relates the number of calculations required of the three approaches with that of no binning. The accuracy compares the mean angle error between the three approaches and no binning as the angle of separation between point clouds increases. The accuracy of the different approaches is also compared by varying the number of bins used.

5.1 Efficiency

To justify the use of binning it is important to confirm that it usefully improves computational performance. When no binning is performed the associated Legendre polynomial (ALP) is the most costly calculation, and is evaluated $(L+1)(L+2)/2$ times for each single normal. The growth rate of the ALP calculations versus degree can be seen in Figure 3a. When binning is employed, the spherical harmonics are pre-computed at the bin centers, shifting the computation to finding which bin a normal belongs too. The three binning approaches are measured in GCD calculations, shown in Figure 3b. The computational time between no binning and binning can be determined from the time required to compute ALP and GCD and the number of times they are each evaluated. For no binning the computational time is ap, where a is the time to calculate ALP per normal and p is the number of normals. The equivalent calculation of binning time is $an + spg$, where n is the number of bins, and s and g are the computational time and number of evaluations of GCD, per normal, respectively. Given $a = 3.3 \times 10^{-3}$ seconds, and $p = 36\,000$, then no binning will take 118.8 seconds. If the Fibonacci spiral binning has 401 bins, $s = 4.9 \times 10^{-7}$ seconds, and on average $g = 10$, then the computational time of the Fibonacci spiral is 1.5 seconds. This shows that binning achieves greater than an order of magnitude improvement in efficiency.

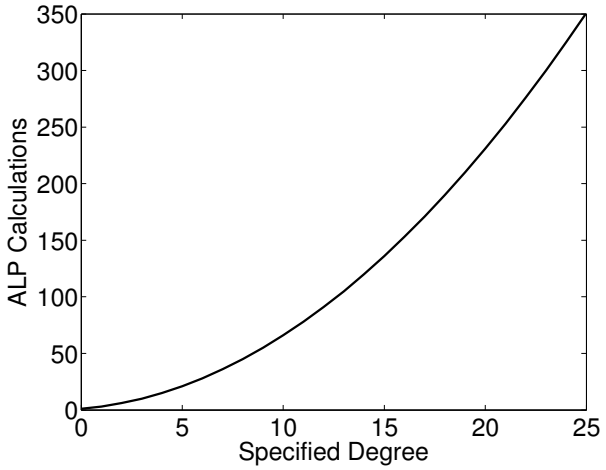

(a) Number of ALP calculations for a specified spherical harmonic degree, normalized per normal.

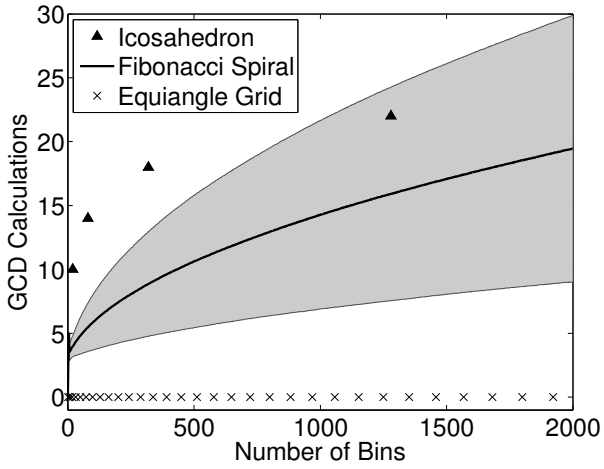

(b) Number of GCD calculations for each of the three binning approaches, where the shaded area is the standard deviation of the Fibonacci Spiral.

Figure 3: Efficiency of the ALP calculations for a given degree, and the efficiency of binning in terms of GCD calculations, when applied to a single normal.

The equiangle grid is the fastest binning approach as it can directly determine which bin a normal belongs without performing a search. When the number of bins is below 1 500 to 2 000, the Fibonacci spiral has the second best performance, with the number of GCD calls for a given normal being dependant on its location. The testing of the Fibonacci spiral is performed by distributing the normals around the sphere using an equiangle distribution, in which $d = 80$ is used. The icosahedron initially has the highest GCD cost, but this is passed by the upper standard deviation of the Fibonacci spiral when the number of bins is approximately 1 000. As the number of bins increases, the icosahedron out performs the Fibonacci spiral, though the point at which this occurs is much greater than the number of bins necessary.

5.2 Accuracy

Binning the normals is shown in the previous section to improve the efficiency of the cross-correlation, however, the achieved accuracy is affected. By varying the number of bins, the trade-off between efficiency and accuracy can be adjusted. Although reducing the number of bins reduces the computational resources required, there is a limit to the minimum number of bins needed to achieve acceptable results. We compare the three binning approaches and identify the number of bins needed to achieve comparable results to no binning. These results are

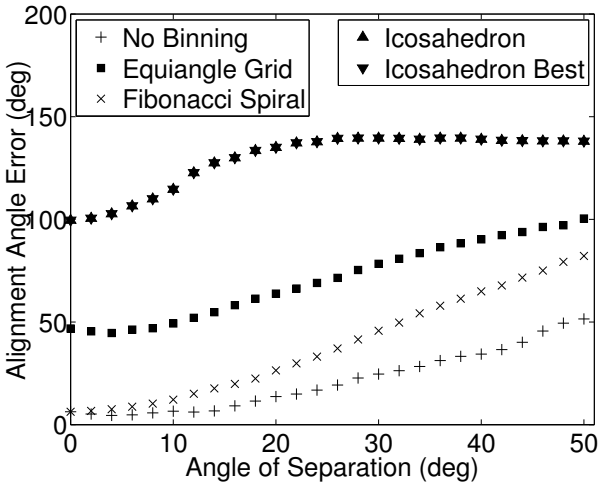

(a) Angle error when using approximately 80 bins.

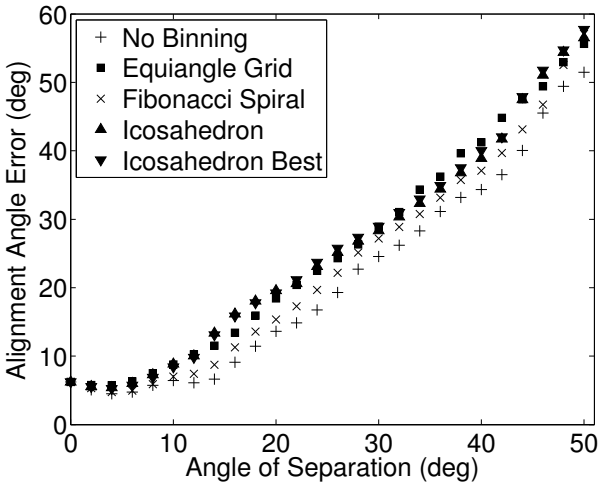

(b) Angle error when using approximately 320 bins.

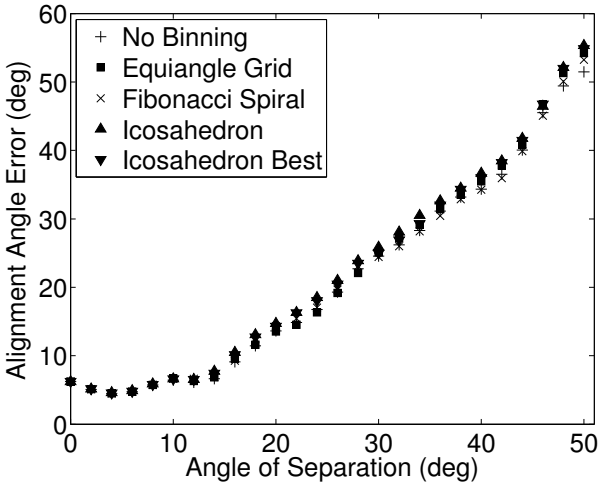

(c) Angle error when using approximately 1260 bins.

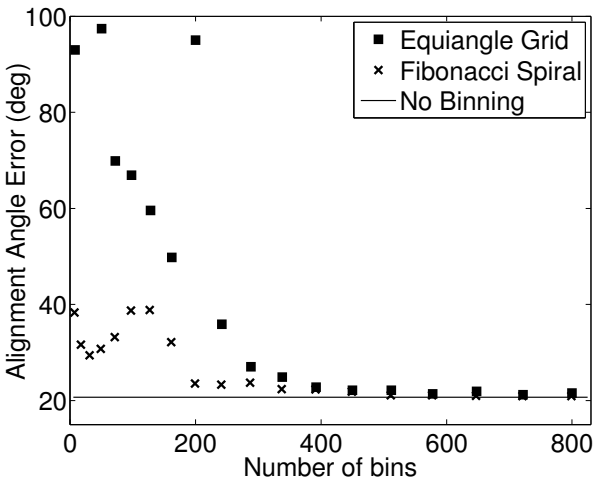

(d) Angle error for all angle separations as the bin count changes.

Figure 4: Alignment error versus the initial angle of separation between two segments; (4a) for approximately 80 bins, (4b) for approximately 320 bins, and (4c) for approximately 1260 bins. Graph (4d) is alignment error versus number of bins when all results of angles of separation are pooled together.

presented in Figure 4. After examining these graphs, it could be concluded that spherical cross-correlation and the binning approaches perform poorly as the angle errors seem rather large. However, it is important to realize that the errors presented are an average of a bimodal distribution, as there are a small number of alignment failures, as discussed further in Section 6. The failed alignments are included in these results to provide a good comparison of the performance between the different binning approaches.

The accuracy was tested using the bin sets in Table 1 to produce Figure 4 which shows how the binning approaches perform in relation to each other and how they compare to no binning at different angles of separation. The icosahedron is tested in two manners, the first (Icosahedron in Figure 4) is the implementation outlined in this paper, and the second (Icosahedron Best in Figure 4) finds the true bin via brute force calculation. There is very little difference in angle error between the two approaches, indicating that the presented implementation is sufficient. Of the three binning approaches the icosahedron has the greatest alignment error, followed by equiangle grid, Fibonacci spiral, and then no binning. The achieved accuracy improves considerably for increased number

of bins, with a performance comparable to that of no binning when over 1000 bins are used. Except when a few bins (~ 80) are used, the angle of separation has a low mean alignment error below 14°, and increases steadily above 14°. This trend occurs for all binning approaches including no binning.

As the comparisons involving the icosahedron approach are limited to a few choices of bins, they do not indicate when the bin count of the equiangle grid and Fibonacci spiral have the same alignment error as no binning. Figure 4d is the relationship between the angle error and the bin count, where each data point is the mean of all angles of separation up to 50°. When fewer than 400 bins are used the alignment error of the Fibonacci spiral is lower than the equiangle grid, and at 199 bins is only 3° higher than no binning. Above 400 bins, the angle error of these two approaches are approximately the same, and slowly decrease, matching no binning at approximately 650 bins.

6. DISCUSSION

The icosahedron binning approach, unexpectedly, has a larger angle error for registration than the equiangle grid. The exact reason is unknown, but may be due to the triangular shape of the bins and how they decrease in size at face edges. The limiting factor of the icosahedron binning, however, is its limited possible number of bins, which does not permit an ideal number of bins to be specified as they grow at a quadratic rate. The second unexpected finding is that the produced results indicate that even though the equiangle approach has a lower density of bins at the equator, this does not have a considerable affect on the cross-correlation performance. This may be due to the robustness of the cross-correlation or that there are a minimal number of normals at the poles. However the equiangle approach is not as stable as the Fibonacci spiral, as misalignments do occur; an example of this is seen in Figure 4d where at 200 bins there is a large outlier. This particular misalignment is likely caused by the placement of bins and how they collect the normals. If the bins collect the normals in a fashion that does not emphasise similar shape between point clouds, the chosen alignment is unlikely to be correct. The opposite effect of this is that the binning emphasises the shape that produces the best alignment, which can be seen for the Fibonacci spiral in Figure 4 when the number of bins is 31.

The spherical cross-correlation attempts to find the rotation that brings the two point clouds into the best alignment. However, if the incorrect rotation is selected and the two point clouds have a form of symmetry, then the selected incorrect rotation will typically produce a misalignment that is out by close to 180°. These large misalignments affect the produced results as the mean angle error is then much higher than what the angle error would be for a correct rotation, thus producing a distribution with a large positive skew. This skew can be seen in Figures 4b and 4c when the angle of separation is greater than 12°; the angle error is seen to grow rapidly due to an increasing number of large misalignments, however, the majority of measured alignments still have a low angle error.

The alignment precision of the spherical cross-correlation is dependant upon the chosen spherical harmonic degree L, where the the number of potential rotations is $(2L+1)^3$. By increasing L the number of selectable rotations increases, thus improving the precision, with some level of error always remaining unless $L = \infty$. Using high values for L is computationally infeasible, so the remaining error makes the spherical cross-correlation a coarse registration algorithm, and is therefore often used in conjunction with the ICP algorithm[14] to produce fine registration. It has been shown that ICP normally achieves registration when the angle of error is below 10°,[15,16] meaning that even if two point clouds do not align correctly using the spherical cross-correlation it is still possible for them to be registered.

7. CONCLUSION

The binning of normals produce a significant decrease in the computational complexity of the spherical cross-correlation as the computation is shifted from calculating spherical harmonics to finding which bin a normal belongs. The Fibonacci spiral, an alternative approach for binning normals was introduced along with an efficient binning implementation. The accuracy and efficiency of the equiangle grid, icosahedron and the Fibonacci spiral binning approaches were compared. The Fibonacci spiral is shown to produce a better accuracy than the equiangle grid and the icosahedron, with an angle error of 3° greater than no binning when 199 bins are used. The equiangle grid has the highest computational efficiency as it can bin a normal directly without searching.

This is followed by the Fibonacci spiral provided the number of bins is less than 1 000, at which point the upper standard deviation of the Fibonacci spiral matches the icosahedron. The cost of binning normals using the Fibonacci spiral is greater than the icosahedron when the number of bins is much greater than necessary. The icosahedron performed poorer than the equiangle grid which was an unexpected and as yet, unexplained result. The introduced Fibonacci spiral is shown to be a beneficial method both in accuracy and efficiency for binning normals in conjunction with the spherical cross-correlation.

ACKNOWLEDGMENTS

The authors gratefully acknowledge the financial support of the University of Waikato Strategic Investment Fund. R.L.L. acknowledges the financial support provided by both the Range Imaging and Waikato Doctoral Scholarships.

REFERENCES

[1] Blais, F., "Review of 20 years of range sensor development," *Journal of Electronic Imaging* **13**, 231–240 (January 2004).

[2] Salvi, J., Matabosch, C., Fofi, D., and Forest, J., "A review of recent range image registration methods with accuracy evaluation," *Image and Vision Computing* **25**(5), 578–596 (2007).

[3] Burel, G. and Henocq, H., "Determination of the orientation of 3D objects using spherical harmonics," *Graphical Models and Image Processing* **57**, 400–408 (September 1995).

[4] Ritchie, D. W. and Kemp, G. J. L., "Fast computation, rotation, and comparison of low resolution spherical harmonic molecular surfaces," *Journal of Computational Chemistry* **20**(4), 383–395 (1999).

[5] Makadia, A., Patterson IV, A., and Daniilidis, K., "Fully automatic registration of 3D point clouds," in [*2006 IEEE Computer Society Conference on Computer Vision and Pattern Recognition*], **1**, 1297–1304 (June 2006).

[6] Shen, L., Huang, H., Makedon, F., and Saykin, A. J., "Efficient registration of 3D SPHARM surfaces," in [*Fourth Canadian Conference on Computer and Robot Vision, 2007. (CRV '07)*], 81–88 (May 2007).

[7] González, A., "Measurement of areas on a sphere using fibonacci and latitude–longitude lattices," *Mathematical Geosciences* **42**, 49–64 (2010).

[8] Saff, E. B. and Kuijlaars, A. B. J., "Distributing many points on a sphere," *The Mathematical Intelligencer* **19**(1), 5–11 (1997).

[9] Teanby, N. A., "An icosahedron-based method for even binning of globally distributed remote sensing data," *Computers & Geosciences* **32**(9), 1442–1450 (2006).

[10] Williamson, D. L., "The evolution of dynamical cores for global atmospheric models," *Journal of the Meteorological Society of Japan* **85B**, 241–269 (2007).

[11] Koay, C. G., "A simple scheme for generating nearly uniform distribution of antipodally symmetric points on the unit sphere," *Journal of Computational Science* (2011). In Press.

[12] Koay, C. G., "Analytically exact spiral scheme for generating uniformly distributed points on the unit sphere," *Journal of Computational Science* **2**(1), 88–91 (2011).

[13] Gutman, B., Wang, Y., Chan, T., Thompson, P. M., and Toga, A. W., "Shape registration with spherical cross correlation," in [*Second MICCAI 2008 Workshop on Mathematical Foundations in Computational Anatomy (MFCA '08)*], 56–67 (2008).

[14] Besl, P. J. and McKay, N. D., "A method for registration of 3-D shapes," *IEEE Transactions on Pattern Analysis and Machine Intelligence* **14**, 239–256 (February 1992).

[15] Larkins, R. L., Cree, M. J., and Dorrington, A. A., "Analysis of ICP variants for the registration of partially overlapping time-of-flight range images," in [*Proceedings of the 25th International Image and Vision Computing New Zealand Conference (IVCNZ 2010)*], (November 2010).

[16] Rusinkiewicz, S. and Levoy, M., "Efficient variants of the ICP algorithm," in [*Proceedings of the Third International Conference on 3-D Digital Imaging and Modeling, 2001*], 145–152 (May 2001).